Light absorption properties of brown carbon aerosol after following the switch from coal to natural gas policy in China: A case study of winter particulate matter over Xi'an, northwestern China

Yukun Chen, Yongwei Lu, Ting Wang, Jukai Chen, Yueshe Wang, Eric Lichtfouse

Atmospheric Pollution Research 14 (2023) 101826

https://doi.org/10.1016/j.apr.2023.101826

Light absorption properties of brown carbon aerosol after following the switch from coal to natural gas policy in China: A case study of winter particulate matter over Xi'an, northwestern China

Yukun Chen [a], Yongwei Lu [a], Ting Wang [a,b], Jukai Chen [a,c], Yueshe Wang [a,*], Eric Lichtfouse [a,d]

[a] State Key Laboratory of Multiphase Flow in Power Engineering, Xi'an Jiaotong University, Xi'an, 710049, China
[b] Xi'an Aeronautics Computing Techniques Research Institute, Xi'an, 710068, China
[c] School of Chemical Engineering & Technology, China University of Mining and Technology, Xuzhou, 221116, PR China
[d] Aix-Marseille University, CNRS, IRD, INRA, Coll France, CEREGE, Aix-en-Provence, 13100, France

ARTICLE INFO

Keywords:
Brown carbon
Coal to natural gas switch policy
Source apportionment
Xi'an
$PM_{2.5}$

ABSTRACT

To control haze pollution, the Xi'an city in northwestern China replaced coal by natural gas in industrial and household heating at the end of 2017. Following this change we studied here the light absorption properties of brown carbon (BrC)in atmospheric particulate matter ($PM_{2.5}$) over Xi'an in 2018. $PM_{2.5}$ samples were collected from November 15 to December 25, 2018, and the light absorption properties of brown carbon in methanol-soluble organic carbon (MSOC) and water-soluble organic carbon (WSOC) were analyzed. Compared to a previous study from the coal combustion period, the mass absorption efficiency (MAE) increased in the sampling period while the radiation-forced absorption fraction of brown carbon relative to elemental carbon reduced, indicating that the light-absorbing capacity and efficiency of brown carbon has improved. Furthermore, highly positive linear relationships ($r > 0.80$) occur between the absorption coefficient and typical products of biomass burning and vehicle emission, except for coal combustion ($r = 0.57$). Additionally, an estimation from the positive matrix factorization and multivariable linear regression model results showed that biomass burning, motor vehicle emission, and secondary source took up approximately 89.53% of $Abs_{WSOC,365}$. The contribution of coal combustion to light absorption BrC was the lowest (7.36% for $Abs_{MSOC,365}$ and 10.24% for $Abs_{WSOC,365}$) in our study, which differs from previous studies in Xi'an. Therefore, the emission source of bulk coal combustion has a relatively small influence on the light absorption of BrC in Xi'an.

1. Introduction

The light absorption properties of atmospheric aerosols play an important role in radiative forcing and visibility (Bond et al., 2013; Li et al., 2019, 2022; Pavel et al., 2023). Black carbon (BC) and mineral dust light-absorbing aerosols that have been researched over the last few decades (Horvath, 1993; Li et al., 2022; Pavel et al., 2023; Sokolik et al., 2001; Wang et al., 2020a). In recent years, studies have shown that brown carbon (BrC, defined as light-absorbing organic aerosol) can absorb radiation efficiently in the near-ultraviolet (UV, 300–400 nm) and visible (Vis) ranges of the light spectrum (Andreae and Gelencsér, 2006; Bond and Bergstrom, 2006; Feng et al., 2013; Xie et al., 2020), while the light-absorption coefficient of BrC has a strong wavelength dependence (λ^{-2}–λ^{-6}), particularly displaying a sharply increasing absorption from Vis to UV ranges (Andreae and Gelencsér, 2006; Feng et al., 2013). Due to its much higher abundance than BC, it has been generally accepted that the role of BrC in atmospheric absorption is significant (Huang et al., 2018; Jiang et al., 2021). In a recent global model study, Lin et al. (2014) estimated that the radiative forcing of BrC accounted for 27–70% of the BC forcing.

Brown carbon can be emitted from primary sources and produced through secondary atmospheric processes (Kasthuriarachchi et al., 2020; Laskin et al., 2015; Yan et al., 2020). The primary sources of BrC have been attributed to forest fires and biomass burning (Chakrabarty et al., 2016; Jiang et al., 2020; Lack et al., 2012; Retama et al., 2022), residential coal combustion and vehicle combustion (Bond et al., 2002; Lei et al., 2018), and biogenic material (Rizzo et al., 2011, 2013). In addition, recent laboratory studies have demonstrated that BrC can be

Peer review under responsibility of Turkish National Committee for Air Pollution Research and Control.
* Corresponding author.
E-mail address: wangys@mail.xjtu.edu.cn (Y. Wang).

generated through heterogeneous reactions and aqueous phase reactions (Bones et al., 2010; Jones et al., 2021; Kampf et al., 2016), which is categorized as 'secondary BrC'. The optical properties of primary BrC from different sources and secondary BrC produced under varied conditions are highly variable (Laskin et al., 2015; Wang et al., 2020a). Several field studies observed temporal and spatial variations in the optical properties of BrC in ambient aerosols (Hoffer et al., 2006; Huang et al., 2018; Liu et al., 2013; Luo et al., 2021; Park et al., 2018; Peng et al., 2020; Singh and Gokhale, 2021), as the sources of BrC are complex and there are mechanisms and factors affecting its atmospheric transformations (Gilardoni et al., 2020; Laskin et al., 2015; Luo et al., 2021).

Brown carbon is widespread in urban regions and its optical properties are affected by emission sources, molecular composition, and the chemistry of light-absorbing components (Jiang et al., 2021; Laskin et al., 2015; Zeng et al., 2020). China's northern cities frenquetly experience severe haze pollution; therefore, emissions-control policies have been established to improve air quality. These policies have been successful to a centain extent (Liu et al., 2019; Wang et al., 2022); however, they might have altered the chemical composition of aerosols, thereby changing aerosol properties. For example, the 2017 coal-to-natural gas switch policy was created because coal combustion for heating was considered a major emission source of particulates and BrC aerosols (Bond et al., 2002; Wang et al., 2020b). In this study, it is speculated that moving away from coal combustion may change the optical properties of atmospheric aerosols in China's northern cities in winter.

Xi'an is one of the megacities in northwestern China where the light absorption properties of BrC were studied before the coal-to-natural gas switch policy (Huang et al., 2018; Lei et al., 2019; Shen et al., 2017c). Huang et al. (2018) investigated BrC in the atmospheric aerosols collected from 2008 to 2009 in the urban area of Xi'an. They claimed that polycyclic aromatic hydrocarbons (PAHs) and their derivatives were observed to be the significant BrC chromophores though the winter, and BrC was attributed mainly to domestic biomass burning. However, PAH emissions are not source-specific but are associated with multiple combustion processes, including biomass burning, coal combustion, and motor vehicle emissions (Shen et al., 2013; Wang et al., 2018; Xie et al., 2019). Furthermore, varoious gaseous and particulate components were emitted during coal combustion. Therefore, the coal control policy may change the chemistry of atmospheric light-absorbing organic compounds (e.g., humic-like substances) contributing to BrC formation.

Based on the previous research, this study focuses on examining the light absorption properties of BrC after the policy, at urban areas of Xi'an. Using the methanol-soluble organic carbon (MSOC) and water-soluble organic carbon (WSOC) to characterize BrC, the influence of changes in BrC emission sources caused by the policy implementation on BrC light absorbance is mainly studied. Specifically, the objectives of this study were to (1) investigate the light absorption characteristics of BrC in winter $PM_{2.5}$ collected in urban Xi'an in 2018; (2) apportion the sources contributing to solvent-extracted BrC; and (3) estimate the fractional contribution of solar absorption by BrC relative to elemental carbon (EC).

2. Methods

2.1. Aerosol sampling

The sampling site is located in an urban area of Xi'an, surrounded by residential areas and heavy traffic roads. More information about the sampling site has been provided in Fig. S1 and Wang et al. (2018). Aerosol sampling was carried out on the roof of a 15 m high building using a CityU $PM_{2.5}$ sampler with a flow rate of 71.3 L min^{-1}. The design, fabrication and validation of the CityU $PM_{2.5}$ sampler has been described in Shen et al. (2017b). Twenty-four-hours samples were collected onto prebaked (780 °C, 5 h) quartz fiber filters (φ = 47 mm, Whatman, UK) from November 15 to December 25, 2018, with a total of 39 filter samples being collected during the campaign. After sampling, all filters were stored in a freezer at −20 °C before analysis.

2.2. Light absorption measurement

2.2.1. Optical properties measurement

The light absorption spectra of water and methanol extracts were measured over a wavelength range of 200–800 nm using a UV-VIS-NIR spectrophotometer (Model Cary 5000, Agilent, US). The recorded spectra were corrected for the filter blanks, and the absorption data (A_λ) were converted to the absorbance coefficient (Abs_λ, Mm^{-1}) of the water or methanol extracts by Eq. (1):

$$Abs_\lambda = (A_\lambda - A_{700})\frac{V_l}{V_a \times L} \times \ln 10 \quad (1)$$

where A_{700} (the absorbance at the wavelength of 700 nm) accounts for baseline shift during analysis, as 700 nm is believed to be free of absorption. V_l (mL) is the volume of solvent (water or methanol) used to extract the filter sample, V_a (m^3) is the volume of air sampled through the filter punch, L (m) is the path length of the cell (1 cm), ln10 is to convert log base-10 (the form provided by spectrophotometer) to a natural logarithm to provide the base-e absorption coefficient (Huang et al., 2018). The average value of absorbance coefficient between 360 nm and 700 nm (Abs_{365}) is used to represent BrC absorption to avoid interferences from certain non-organic components and maintain consistency with previously reported results (Hecobian et al., 2010; Huang et al., 2018).

The wavelength dependence of the light absorption by chromophores in a solution can be described by Eq. (2):

$$Abs_\lambda = k \times \lambda^{-AAE} \quad (2)$$

where k is a constant related to the concentration of chromophores. *AAE* is the absorption Angstrom exponent of the soluble extracts, representing a measure of the variation of the light absorption of BrC with wavelength, that is, the dependence on the wavelength. In this study, *AAE* is determined by a linear regression of $\log Abs_\lambda$ versus $\log\lambda$ in the wavelength range from 330 nm to 550 nm.

The mass absorption efficiency (*MAE*, $m^2 \cdot g^{-1}$) of the filter extract at a given wavelength can be calculated by Eq. (3):

$$MAE_\lambda = \frac{Abs_\lambda}{M_i} \quad (3)$$

where M_i is the mass concentration of WSOC or MSOC ($\mu gC \cdot m^{-3}$). The *MAE* represents the light absorption efficiency of BrC, which is defined as the light absorption intensity of brown carbon per unit mass. Characterizing the optical properties of BrC is a major parameter.

2.2.2. Radiative forcing absorbed by BrC relative to elemental carbon (EC)

The fraction of solar radiation BrC absorbed directly relative to EC in a particular wavelength range (300–2500 nm, 300–700 nm and 300–400 nm in this case) can be described by Eq. (4) (Lei et al., 2018). Using numerical simulation, a model was used to compute the proportion of every sample in MATLAB version 2013b. Two assumptions made by Huang et al. (2018) were adopted. The radiative forcing on the ground can be used to characterize the atmospheric boundary layer, and the light absorption coefficient of soluble BrC in MSOC and WSOC is consistent with the granular BrC in the atmosphere.

$$f = \frac{\int I_0(\lambda)\left\{1 - e^{-MAC_{365}\left(\frac{365}{\lambda}\right)^{AAE_{WSOC/MSOC}} \times C_{WSOC/MSOC} \times h_{ABL}}\right\} d\lambda}{\int I_0(\lambda)\left\{1 - e^{-MAC_{632}\left(\frac{632}{\lambda}\right)^{AAE_{EC}} \times C_{EC} \times h_{ABL}}\right\} d\lambda} \quad (4)$$

In Eq. (4), λ is the wavelength, and $I_0(\lambda)$ is the solar irradiance measured on the ground. Generally, the I_0 can be calculated in the whole

wavelength range using the clear sky air mass 1 global horizontal (AM1GH) irradiance model established by Levinson et al. (2010). MAC_{365} represents the mass absorption coefficient of BrC at 365 nm, describing the absorption capacity of granular light-absorbing components. Similarly, MAC_{632} correspond to the mass absorption coefficient of EC at 632 nm. From hereon, we used the value of 8.45 m^2 g^{-1} as published by Cheng et al. (2011). The *AAE* of MSOC or WSOC can be calculated by Eq. (2) in Section 2.2.1. The *AAE* of EC is considered to be 1 as it is a wavelength-independent material and absorbs solar light over the whole solar spectrum. $C_{WSOC/MSOC}$ and C_{EC} are the concentrations of WSOC, MSOC and EC obtained by the analyzing water-soluble ions and carbonaceous fractions, respectively, and details canb be obtained in the supplement. h_{ABL} is the height of atmospheric boundary layer. As the effects on the calculation from 300 m to 2000 m are low, the value of 1000 m was chosen, as reported by Kirillova et al. (2014).

However, the *AAE* for ambient particles (measured between a short and long visible wavelength) has often been observed to be larger than 1. As known, most of AAE_{EC} in published literatures was assumed to be 1 (Andersson, 2017; Choudhary et al., 2018; Pavel et al., 2023). However, some published literatures were focused on the light absorption of elemental carbon or black carbon. The absorption Ångström exponent (*AAE*) for externally mixed black carbon (BCExt) is predicted to be wavelength-independent ($AAE = 1$) for particles <50 nm diameter (Lack and Langridge, 2013). A recent study also suggested a lower limit of $AAE = 0.55$ for atmospheric "elemental carbon" (a term functionally similar to BC) (Bahadur et al., 2012; Lack and Langridge, 2013). Additionally, for example, Wang et al. (2020a) reported that the AAE_{BC} was equal to 1.19 within the range of 0.6–1.6 published data. The AAE_{BC} at the sampling location was found to be 1.1 ± 0.05 (Rathod and Sahu, 2022). Furthermore, The AAE of aggregates with different size distributions vary between 0.87 and 1.50, whereas those of the spheres or spheroids have wider ranges (Li et al., 2016). And Luo et al. (2020) calculated the AAE was in the range of 0.6–1.2 for BC with non-absorbing coatings is generally consistent with the observed range of Kirchstetter et al. (2004), who obtained a BC *AAE* range of 0.6–1.3. Thus, in the study, our assumption that AAE_{EC} equals 1 is consistent with the traditional assumption and falls within the range of experimental measurements and numerical simulations in the published literatures.

2.3. Positive matrix factorization (PMF) analysis

The PMF model (EPA PMF 5.0) was used to resolve potential sources and apportion their contribution to atmospheric levels of WSOC and MSOC. A detailed description of the PMF 5.0 application on source apportionment can be found in Fundamentals and User Guide (https://www.epa.gov/sites/production/files/2015-02/documents/pmf_5.0_user_guide.pdf). OC, EC, seven water-soluble ions and $PM_{2.5}$ were applied for the model input. The uncertainties of each species were calculated using Eq. (5):

$$Unc = \sqrt{(EF * Con)^2 + (0.5 * MDL)^2} \quad (5)$$

where *Con* is the concentration of each species, and *EF* is the error fraction, representing the proportion of the error to the concentration of the analyzed components. *EF*Con* represents the uncertainty associated with the concentration of the components, mainly from the error in the sample analysis. In each experiment, measurement were repeated for every ten samples tested. The concentration error was within a fixed range (10% for WSOC, MSOC and EC, 5% for water-soluble ions). As for $PM_{2.5}$, *EF* is defined as the detection limit of the weighting system divided by the minimum value of $PM_{2.5}$ mass concentration. *MDL* is the method detection limit, which depends on the instruments used in the measurement.

The PMF model was run with 4–7 factors and random seeds. The 5-factor model was considered optimal based on the *Q* values (the weighted least-squares of differences between the observations and the model) and the interpretable factors identified by PMF. All the scaled residuals were between ±3, with >90% between ±1 in our case. Although lower *Q* values and scaled residuals could be obtained when adding more factors, it did not result in much improvement when interpreting the factor profiles based on the references for sources of atmospheric $PM_{2.5}$ in Xi'an (Cao et al., 2012; Huang et al., 2014; Wang et al., 2015).

2.4. Source apportionment of the light absorption coefficient of BrC in MSOC and WSOC

According to Section 2.3, the potential sources contributing to BrC can be obtained. Quantitative analysis can then be used to ensure the contribution of every source to $Abs_{MSOC,365}$ and $Abs_{WSOC,365}$ was established. The method can be referred to Lei et al. (2018) using the multivariable linear regression model shown in Eq. (6):

$$Abs_{MSOC/WSOC,365} = B + \sum_{i,j=1}^{n} A_i \times [X_{ij}] \quad (6)$$

where *i* and *j* are the *i*-th factor and the *j*-th day in our case, respectively. $[X_{ij}]$ is the contribution of the *i*-th factor on the *j*-th day. This result can be obtained by PMF analysis. A_i is the regression coefficient. $A_i \times [X_{ij}]$ means the predicted light absorption coefficient of MSOC or WSOC by the linear regression model. *B* represents the random error in the model. $Abs_{MSOC/WSOC,365}$ is the actual value we measured in Section 2.2.1.

3. Results and discussion

To thoroughly investigate whether the 2017 coal-to-natural gas policy switch has changed the aerosol properties and sources in Xi'an, this experiment focused on studying the change in optical properties and sources of organic carbon aerosols after the policy and comparing the experimental results with previous studies. The results are described below.

3.1. Light absorption properties of BrC

Fig. 1 shows the daily variation in the average light absorption coefficient of BrC in MSOC and WSOC ($Abs_{MSOC,365}$ and $Abs_{WSOC,365}$, respectively) and the concentration of MSOC and WSOC in this study (a) and in a previous study (b) (Lei et al., 2019). Since the optical properties of WSOC are not depicted in Lei's study (2019), only the light absorption characteristics of MSOC are compared here. As shown in Fig. 1(a), the concentrations of MSOC and WSOC have strong synergies with the corresponding average light absorption coefficient at a wavelength of 365 nm ($Abs_{MSOC,365}$ and $Abs_{WSOC,365}$). $Abs_{MSOC,365}$ is about twice (1.9) as high as $Abs_{WSOC,365}$, suggesting that MSOC can better characterize BrC than WSOC. The concentration of MSOC in this study (Fig. 1(a)) is much lower than that of previous studies in which OC characterizes MSOC (Fig. 1(b)), impling a decrease in the concentration of light-absorbing BrC. Fig. 1(b) shows the daily varination in average light absorption coefficient of MSOC ($Abs_{MSOC,365}$) in previous study (Lei et al., 2019). Compared to the previous policy result of $Abs_{MSOC,365}$ being equal to 42.0 ± 18.1 Mm^{-1} (Fig. 1(b)), we observed the average $Abs_{MSOC,365}$ value (33.0 ± 17.1 Mm^{-1}) had decreased, indicating a slight reduction in light absorption intensity of BrC following the coal control policy. Furthermore, it has been proven that this policy may weaken the occurrence of haze phenomenon and effectively modify environmental quality.

The *AAE* value, representing the dependence of the light absorption capacity of BrC on wavelengths from 330 nm to 550 nm, can be obtained by logarithmic fitting of the light absorption coefficient and wavelength. In this study, the AAE_{MSOC} is 6.8 ± 0.04 (Table S1), slightly higher than the prior value (6.2 ± 0.5). This result indicates that the absorption capacity of BrC is more dependent on the wavelength after the policy.

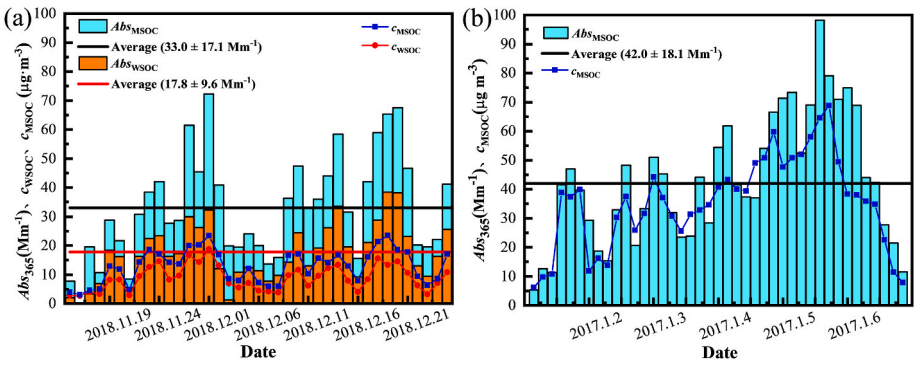

Fig. 1. The daily variation of average light adsorption coefficient of brown carbon (BrC) in methanol-soluble organic carbon (MSOC) and water-soluble organic carbon (WSOC) ($Abs_{MSOC,365}$ and $Abs_{WSOC,365}$, respectively) and MSOC and WSOC in this study (a) and Lei et al. (2019) (b).

According to the published literature by Yan et al. (2018), when the *AAE* value is higher than 3, the primary and secondary BrC may originate from biomass burning emissions.

Fig. 2 shows the daily average *MAE* of BrC at 365 nm in our study (a) and the previous study (b). In our study, the average *MAE* values of BrC in MSOC ($MAE_{MSOC,365}$) and WSOC at 365 nm ($MAE_{WSOC,365}$) are 2.5 ± 0.5 m^2 g^{-1} and 2.0 ± 0.6 m^2 g^{-1}, respectively. At the same time, the $MAE_{MSOC,365}$ was 1.2 ± 0.2 m^2 g^{-1} in the previous study. As a major parameter to characterize the light absorption intensity of BrC, the results from the *MAE* calculation formula show that the light absorption intensity of BrC per unit mass has increased in the winter in Xi'an following the policy. However, the concentration of BrC in this experiment is much lower than that in previous studies. This phenomenon may be due to more light-absorbing components in BrC at a lower ultraviolet wavelength.

Table S1 collates the average optical parameters (Abs_{365}, MAE_{365} and *AAE*) of BrC in this study and those reported in different regions during winter. The Abs_{365} and *AAE* values in our case are all within the scope of other studies. However, the MAE_{365} and *AAE* of MSOC and WSOC in Xi'a are higher than in other regions, and the possible cause resulting in these phenomena is the different types and quantities of light-absorbing BrC in Xi'an. Regarding the light absorption parameters of BrC (Huang et al., 2018; Shen et al., 2017c), the average Abs_{365} values in this study (methanol-soluble BrC: 33.0 ± 17.1 Mm^{-1}; water-soluble BrC: 17.8 ± 9.6 Mm^{-1}) are slightly lower than previously reported values. Nevertheless, MAE_{365} is approximately two times higher than previous results. These illustrate an increase in the light-absorbing ability and efficiency of BrC after the policy. Thus, it is speculated that the relative contribution to light-absorbing BrC from different emission sources has been changed by the implementation of the policy.

Since variations in chemical components can represent different emission sources, a correlation analysis between the light absorption coefficient ($Abs_{MSOC,365}$ and $Abs_{WSOC,365}$) and several representative species is conducted to preliminarily predict the emission sources leading to the light absorption of BrC. Fig. 3 shows the linear correlation coefficient (r) between the light absorption coefficient and the mass concentration of different typical species. There are strong correlations between Abs_{365} and K^+ (r = 0.95 for $Abs_{MSOC,365}$, r = 0.93 for $Abs_{WSOC,365}$), OC1 (r = 0.88 for $Abs_{MSOC,365}$, r = 0.89 for $Abs_{WSOC,365}$) and OC2 (r = 0.87 for both $Abs_{MSOC,365}$ and $Abs_{WSOC,365}$), which are the characteristic of biomass burning (Shen et al., 2017a), implying that this is an important emission source to BrC. Furthermore, an appropriate correlation was observed for both EC (r = 0.88 for $Abs_{MSOC,365}$, r = 0.82 for $Abs_{WSOC,365}$) and NO_3^- (r = 0.80 for $Abs_{MSOC,365}$, r = 0.89 for $Abs_{WSOC,365}$). Both diesel and gasoline combustion produce large amounts of EC and NOx (Yao et al., 2016); hence, motor vehicle emissions can be identified as another important emission source.

In contrast, the correlation coefficient r between Abs_{365} and SO_4^{2-} is realtively low (0.57). SO_4^{2-} is formed by the transformation of SO_2 in the atmosphere, which is mainly sourced from coal combustion. The low correlation coefficients imply that the contribution from coal combustion is not as significant as that from biomass burning and motor vehicles during our sampling period. However, previous studies showed that coal combustion is important for generating BrC. Shen et al. (2017c) collected coal combustion samples over Xi'an during the winter (from 15 November 2008, to 14 March 2009) to identify the contribution to BrC. They reported that the average values of Abs_{340} and *AAE* of BrC were 84.9 Mm^{-1} and 4.38, respectively, and the *AAE* value of ambient samples in a simultaneous period was between those from coal combustion and biomass burning, concluding that coal combustion was one of the main contributors. In addition, after studying the source apportionment of BrC in winter (from 19 December 2015, to 1 January 2016)

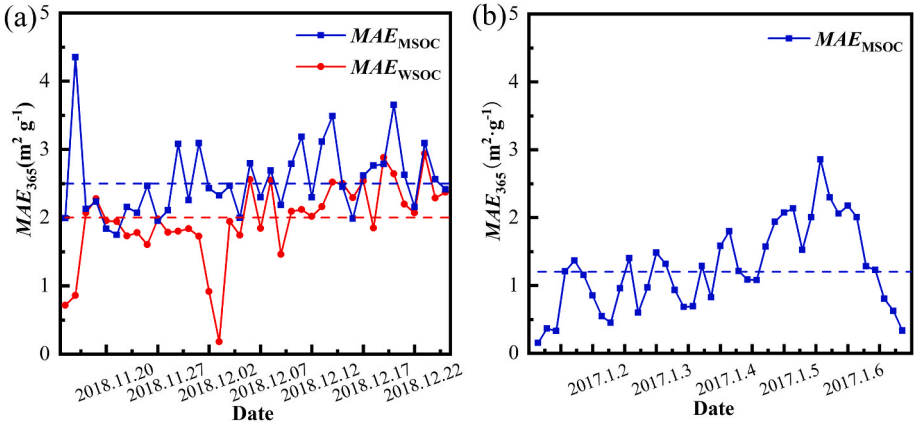

Fig. 2. The daily mass absorption efficiency at 365 nm (MAE_{365}) of BrC in MSOC (blue curve) and WSOC (red curve) in this study (a) and Lei et al. (2019) (b).

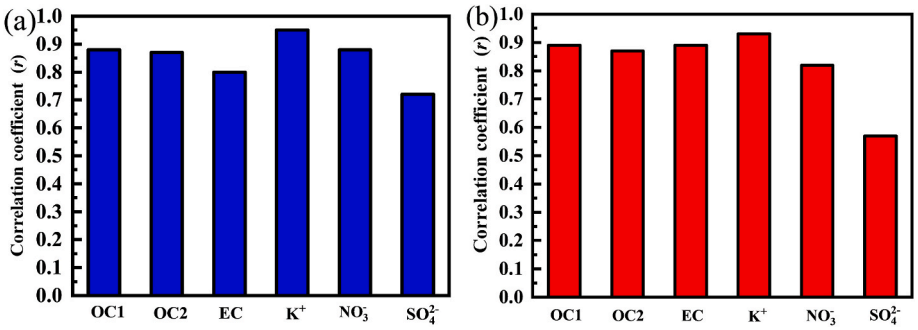

Fig. 3. The linear correlation coefficient (r) between the abundance of typical species (OC1, OC2, EC, K^+, NO_3^-, and SO_4^{2-}) and $Abs_{365,MSOC}$ (a) and $Abs_{365,WSOC}$ (b).

using daily $PM_{2.5}$ samples over Yulin, a city near to Xi'an, Lei et al. (2018) reported coal combustion was an essential source to BrC resulting from the high correlation coefficient between $Abs_{MSOC,365}$ and typical carbon fractions, and PAHs. They considered that the proportion of coal combustion emissions to $Abs_{MSOC,365}$ was 42.9%, indicating the BrC emitted from the coal combustion was a significant contributor. In contrast, the low linear relationship between Abs_{365} and SO_4^{2-} in this study suggests that coal combustion is likely to have only a small contribution to BrC after the control policy has been implemented. Evidence of source apportionment results will support this speculation in the next section.

3.2. Source apportionment of BrC in WSOC and MSOC

The source apportionment of $PM_{2.5}$ and their contribution to OC during winter at Xi'an are shown in Fig. S2. Five emission sources resulted in pollution, such as biomass burning, motor vehicle emissions, coal combustion, dust, and secondary source. The detailed identification of the five factors is illustrated in the supplemental information.

Furthermore, the contribution from the different sources to the light absorption coefficient is quantified using the multivariable linear regression model. The pie charts in Fig. 4 show the proportion of main contributors to $Abs_{MSOC,365}$ (a) and $Abs_{WSOC,365}$ (b) during the winter in Xi'an. Although the dust sources were not included, four sources were identified, resulting from the extracted solution handled by 0.22 μm filters (Lei et al., 2018). In general, the components in dust are almost insoluble; therefore, it is not considered a contributor to the light absorption coefficient. Besides these four sources, certain humic-like substances (HULIS) and alkaline soluble organic carbon (ASOC) from other sources, like bioaerosols in the water or methanol extracts, can absorb solar radiation (Li et al., 2018).

As shown in Fig. 4, biomass burning, motor vehicle emissions, and secondary source, are the main contributors to both $Abs_{MSOC,365}$ and $Abs_{WSOC,365}$, accounting for around 72.60% and 89.53%, respectively. For the optical properties of BrC from MSOC (Fig. 4(a)), the secondary source is the main contributor, accounting for 39.4%. The second contribution is biomass burning (21.27%), followed by motor vehicle emissions (11.93%). The contribution of coal combustion to $Abs_{MSOC,365}$ is the lowest, only accounting for 7.36%. A slight difference in the contribution to the light absorption coefficient of BrC from WSOC compared to that of MSOC was observed. The highest contribution is biomass burning (36.26%), followed by motor vehicle emissions (27.75%). As secondary reactions mainly produceWSOC, the BrC in WSOC from the secondary source is also important, accounting for 25.52%. Again, the contribution from coal combustion is the lowest, only accounting for 10.24%.

3.3. Evaluation of radiative forcing by BrC relative to EC

Although EC is the dominate light-absorbing carbon species in the solar spectrum, BrC is a crucial component at the wavelength of ultraviolet–visible (from 300 nm to 400 nm) range to absorb solar radiation. In order to indicate the contribution portion of the light-absorbing species, BrC, the average radiative forcing fraction of MSOC and WSOC relative to EC during winter in Xi'an was calculated (Fig. 5). The average radiation forcing by MSOC/EC is larger than that by WSOC/EC. This is because the solar absorption fraction of MSOC/EC and WSOC/EC increases from the whole solar spectrum (300–2500 nm) to just the UV range (300–400 nm). As BrC has strong light absorption in the UV and near UV wavelength ranges, we will only discuss the results in the UV range. As shown in Fig. 5, the average radiation forcing fractions of MSOC/EC (Fig. 5(a)) and WSOC/EC (Fig. 5(b)) in the UV range were 53.56% and 28.11%, respectively. In contrast, the values of MSOC/EC and WSOC/EC in the previous study are 76% and 42%, respectively, larger than the results in our studies. These differences may indicate that since the ability and efficiency of BrC have increased according to the results in Section 3.1, the abundance of BrC has decreased after the policy of swapping coal for natural gas.

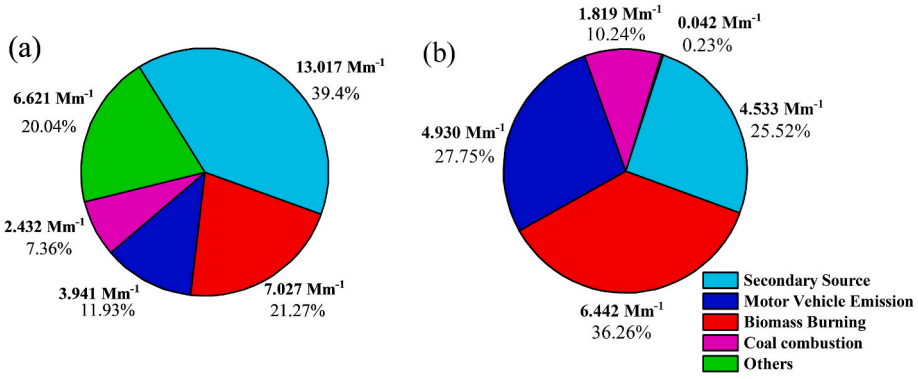

Fig. 4. The source contribution to $Abs_{MSOC,365}$ (a) and $Abs_{WSOC,365}$ (b) using a multivariate linear regression model.

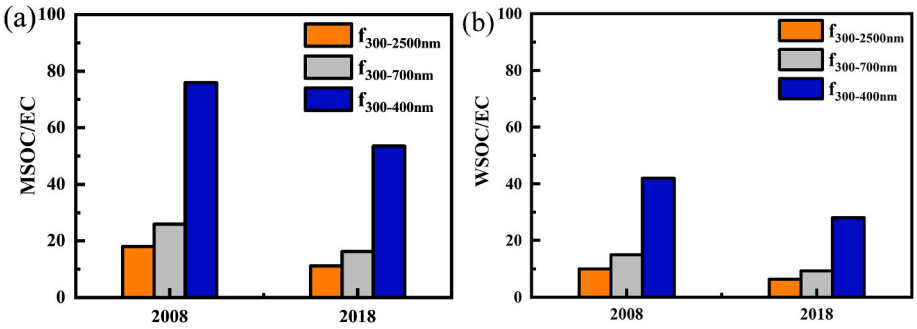

Fig. 5. The average radiative forcing absorbed by BrC in MSOC (a) and WSOC (b) relative to EC in different wavelength ranges during winter in Xi'an between this and Huang et al. (2018).

4. Conclusion

In this study, we focused on the light-absorbing organic compounds in $PM_{2.5}$ in Xi'an, comparing the impact on the light absorption properties and emission sources of the BrC before and after implementating the coal-to-gas switch policy. The average *Abses* of MSOC and WSOC at 365 nm were 33.0 ± 17.1 Mm^{-1} and 17.8 ± 9.6 Mm^{-1}, respectively, which were slightly lower than those from the previous values before the coal control policy. However, the *AAEs* of MSOC (6.8 ± 0.04) and WSOC (6.1 ± 0.05) in the wavelength from 330 nm to 550 nm showed a rising trend after the policy, and this means that in the low wavelength range of visible to ultraviolet lights, the light absorption of BrC is more wavelength dependent. The average *MAEs* of MSOC and WSOC at 365 nm were 2.5 ± 0.5 $m^2\ g^{-1}$ and 2.0 ± 0.6 $m^2\ g^{-1}$. Both have increased compared to the previous study, indicating an increase in the light-absorbing efficiency of BrC. We then evaluated the solar radiative forcing of BrC relative to EC from the whole wavelength range to the UV range. The results showed that the average radiative forcing of BrC in MSOC or WSOC relative to one of ECs reached to 53.56% and 28.11% in the UV range. Compared to the results prior to the implementation of the coal-control policy, the radiative forcing fraction was reduced. The BrC absorbed less solar radiation but was more efficient at absorbing light. This phenomenon is likely to be attributed to changes in the light-absorbing properties of BrC.

By analyzing the synergy between the typical species (OC1, OC2, EC, and ions) from possible emission sources and the absorption coefficient, we observed that the representative products had an excellent linear relationship with $Abs_{MSOC,365}$ and $Abs_{WSOC,365}$ (except SO_4^{2-}). After, the original inference that the coal-to-natural gas policy may change the contribution of coal combustion to BrC and the light absorption properties of BrC, the PMF results also confirmed this hypothesis. Five emission sources to BrC were observed, and the contribution from coal combustion was the lowest. The main contributors were biomass burning, motor vehicle emissions, and secondary source, accounting for 72.60% (24.0 Mm^{-1}) and 89.53% (15.9 Mm^{-1}) to $Abs_{MSOC,365}$ and $Abs_{WSOC,365}$, respectively. Therefore, this policy only turns off the emission sources that have had the least impact on the light absorption of BrC. Overall, based on our findings, follow-up studies are suggested to identify the key components in biomass burning, motor vehicle emissions, and secondary source that contribute to BrC, aiming to find an effective way of reducing the light-absorbing ability of BrC.

Credit author statement

Yukun Chen: Conceptualization, Methodology, Writing- Original draft preparation. **Yongwei Lu.**: Data curation, Software, Formal analysis., **Ting Wang**: Visualization, Investigation. **Jukai Chen**: Writing - Review & Editing, Methodology, Resources. **Yueshe Wang**: Supervision. Writing- Reviewing and Editing, Funding acquisition. **Eric Lichtfouse**: Software, Validation.

Declaration of competing interest

The authors declare that they have no known competing financial interests or personal relationships that could have appeared to influence the work reported in this paper.

Acknowledgments

This work was supported by the National Natural Science Foundation of China (grant numbers 51576160 and 52206215) and Program of the Ministry of Education of China (grant numbers BP0719017). Our acknowledgment also goes to the State Key Laboratory of Multiphase Flow in Power Engineering of Xi'an Jiaotong University for providing measuring apparatus. The authors would like to express gratitude to the anonymous reviewers who supplied valuable feedback toward improving this manuscript.

Appendix A. Supplementary data

Supplementary data to this article can be found online at https://doi.org/10.1016/j.apr.2023.101826.

References

Andersson, A., 2017. A model for the spectral dependence of aerosol sunlight absorption. ACS Earth and Space Chemistry 1 (9), 533–539. https://doi.org/10.1021/acsearthspacechem.7b00066.

Andreae, M.O., Gelencsér, A., 2006. Black carbon or brown carbon? The nature of light-absorbing carbonaceous aerosols. Atmos. Chem. Phys. 6 (10), 3131–3148.

Bahadur, R., Praveen, P.S., Xu, Y., Ramanathan, V., 2012. Solar absorption by elemental and brown carbon determined from spectral observations. Proc. Natl. Acad. Sci. U. S. A. 109 (43), 17366–17371. https://doi.org/10.1073/pnas.1205910109.

Bond, T.C., Bergstrom, R.W., 2006. Light absorption by carbonaceous particles: an investigative review. Aerosol. Sci. Technol. 40 (1), 27–67. https://doi.org/10.1080/02786820500421521.

Bond, T.C., Covert, D.S., Kramlich, J.C., Larson, T.V., Charlson, R.J., 2002. Primary particle emissions from residential coal burning: optical properties and size distributions. J. Geophys. Res. Atmos. 107 (D21) https://doi.org/10.1029/2001jd000571.

Bond, T.C., Doherty, S.J., Fahey, D.W., Forster, P.M., Berntsen, T., DeAngelo, B.J., Zender, C.S., 2013. Bounding the role of black carbon in the climate system: a scientific assessment. J. Geophys. Res. Atmos. 118 (11), 5380–5552. https://doi.org/10.1002/jgrd.50171.

Bones, D.L., Henricksen, D.K., Mang, S.A., Gonsior, M., Bateman, A.P., Nguyen, T.B., Nizkorodov, S.A., 2010. Appearance of strong absorbers and fluorophores in limonene-O3secondary organic aerosol due to NH4+-mediated chemical aging over long time scales. J. Geophys. Res. 115 (D5) https://doi.org/10.1029/2009jd012864.

Cao, J.-j., Wang, Q.-y., Chow, J.C., Watson, J.G., Tie, X.-x., Shen, Z.-x., An, Z.-s., 2012. Impacts of aerosol compositions on visibility impairment in Xi'an, China. Atmos. Environ. 59, 559–566. https://doi.org/10.1016/j.atmosenv.2012.05.036.

Chakrabarty, R.K., Gyawali, M., Yatavelli, R.L.N., Pandey, A., Watts, A.C., Knue, J., Moosmüller, H., 2016. Brown carbon aerosols from burning of boreal peatlands: microphysical properties, emission factors, and implications for direct radiative forcing. Atmos. Chem. Phys. 16 (5), 3033–3040. https://doi.org/10.5194/acp-16-3033-2016.

Cheng, Y., He, K.B., Zheng, M., Duan, F.K., Du, Z.Y., Ma, Y.L., Russell, A.G., 2011. Mass absorption efficiency of elemental carbon and water-soluble organic carbon in

Beijing, China. Atmos. Chem. Phys. 11 (22), 11497–11510. https://doi.org/10.5194/acp-11-11497-2011.
Choudhary, V., Rajput, P., Singh, D.K., Singh, A.K., Gupta, T., 2018. Light absorption characteristics of brown carbon during foggy and non-foggy episodes over the Indo-Gangetic Plain. Atmos. Pollut. Res. 9 (3), 494–501. https://doi.org/10.1016/j.apr.2017.11.012.
Feng, J., Li, M., Zhang, P., Gong, S., Zhong, M., Wu, M., Lou, S., 2013. Investigation of the sources and seasonal variations of secondary organic aerosols in PM2. 5 in Shanghai with organic tracers. Atmos. Environ. 79, 614–622.
Gilardoni, S., Massoli, P., Marinoni, A., Mazzoleni, C., Freedman, A., Lonati, G., Gianelle, V., 2020. Spatial and temporal variability of carbonaceous aerosol absorption in the Po valley. Aerosol Air Qual. Res. 20 (12), 2624–2639. https://doi.org/10.4209/aaqr.2020.03.0085.
Hecobian, A., Zhang, X., Zheng, M., Frank, N., Edgerton, E.S., Weber, R.J., 2010. Water-Soluble Organic Aerosol material and the light-absorption characteristics of aqueous extracts measured over the Southeastern United States. Atmos. Chem. Phys. 10 (13), 5965–5977. https://doi.org/10.5194/acp-10-5965-2010.
Hoffer, A., Gelencsér, A., Guyon, P., Kiss, G., Schmid, O., Frank, G., Andreae, M., 2006. Optical properties of humic-like substances (HULIS) in biomass-burning aerosols. Atmos. Chem. Phys. 6 (11), 3563–3570.
Horvath, H., 1993. Atmospheric light absorption—a review. Atmos. Environ., Part A 27 (3), 293–317. https://doi.org/10.1016/0960-1686(93)90104-7.
Huang, R.J., Yang, L., Cao, J., Chen, Y., Chen, Q., Li, Y., Dusek, U., 2018. Brown carbon aerosol in urban xi'an, northwest China: the composition and light absorption properties. Environ. Sci. Technol. 52 (12), 6825–6833. https://doi.org/10.1021/acs.est.8b02386.
Huang, R.J., Zhang, Y., Bozzetti, C., Ho, K.F., Cao, J.J., Han, Y., Prevot, A.S., 2014. High secondary aerosol contribution to particulate pollution during haze events in China. Nature 514 (7521), 218–222. https://doi.org/10.1038/nature13774.
Jiang, H., Li, J., Chen, D., Tang, J., Cheng, Z., Mo, Y., Zhang, G., 2020. Biomass burning organic aerosols significantly influence the light absorption properties of polarity-dependent organic compounds in the Pearl River Delta Region, China. Environ. Int. 144, 106079 https://doi.org/10.1016/j.envint.2020.106079.
Jiang, H., Li, J., Sun, R., Tian, C., Tang, J., Jiang, B., Zhang, G., 2021. Molecular dynamics and light absorption properties of atmospheric dissolved organic matter. Environ. Sci. Technol. 55 (15), 10268–10279. https://doi.org/10.1021/acs.est.1c01770.
Jones, S.H., Friederich, P., Donaldson, D.J., 2021. Photochemical aging of levitated aqueous Brown carbon droplets. ACS Earth and Space Chemistry 5 (4), 749–754. https://doi.org/10.1021/acsearthspacechem.1c00005.
Kampf, C.J., Filippi, A., Zuth, C., Hoffmann, T., Opatz, T., 2016. Secondary brown carbon formation via the dicarbonyl imine pathway: nitrogen heterocycle formation and synergistic effects. Phys. Chem. Chem. Phys. 18 (27), 18353–18364. https://doi.org/10.1039/c6cp03029g.
Kasthuriarachchi, N.Y., Rivellini, L.H., Adam, M.G., Lee, A.K.Y., 2020. Light absorbing properties of primary and secondary Brown carbon in a tropical urban environment. Environ. Sci. Technol. 54 (17), 10808–10819. https://doi.org/10.1021/acs.est.0c02414.
Kirchstetter, T.W., Novakov, T., Hobbs, P.V., 2004. Evidence that the spectral dependence of light absorption by aerosols is affected by organic carbon. J. Geophys. Res. Atmos. 109 (D21) https://doi.org/10.1029/2004jd004999 n/a-n/a.
Kirillova, E.N., Andersson, A., Tiwari, S., Srivastava, A.K., Bisht, D.S., Gustafsson, Ö., 2014. Water-soluble organic carbon aerosols during a full New Delhi winter: isotope-based source apportionment and optical properties. J. Geophys. Res. Atmos. 119 (6), 3476–3485. https://doi.org/10.1002/2013jd020041.
Lack, D.A., Langridge, J.M., 2013. On the attribution of black and brown carbon light absorption using the Ångström exponent. Atmos. Chem. Phys. 13 (20), 10535–10543. https://doi.org/10.5194/acp-13-10535-2013.
Lack, D.A., Langridge, J.M., Bahreini, R., Cappa, C.D., Middlebrook, A.M., Schwarz, J.P., 2012. Brown carbon and internal mixing in biomass burning particles. Proc. Natl. Acad. Sci. U. S. A. 109 (37), 14802–14807. https://doi.org/10.1073/pnas.1206575109.
Laskin, A., Laskin, J., Nizkorodov, S.A., 2015. Chemistry of atmospheric brown carbon. Chem. Rev. 115 (10), 4335–4382. https://doi.org/10.1021/cr5006167.
Lei, Y., Shen, Z., Wang, Q., Zhang, T., Cao, J., Sun, J., Wu, J., 2018. Optical characteristics and source apportionment of brown carbon in winter PM 2.5 over Yulin in Northern China. Atmos. Res. 213, 27–33. https://doi.org/10.1016/j.atmosres.2018.05.018.
Lei, Y., Shen, Z., Zhang, T., Lu, D., Zeng, Y., Zhang, Q., Cao, J., 2019. High time resolution observation of PM2.5 Brown carbon over Xi'an in northwestern China: seasonal variation and source apportionment. Chemosphere 237, 124530. https://doi.org/10.1016/j.chemosphere.2019.124530.
Levinson, R., Akbari, H., Berdahl, P., 2010. Measuring solar reflectance—Part I: defining a metric that accurately predicts solar heat gain. Sol. Energy 84 (9), 1717–1744. https://doi.org/10.1016/j.solener.2010.04.018.
Li, J., Liu, C., Yin, Y., Kumar, K.R., 2016. Numerical investigation on the Ångström exponent of black carbon aerosol. J. Geophys. Res. Atmos. 121 (7), 3506–3518. https://doi.org/10.1002/2015jd024718.
Li, M., Fan, X., Zhu, M., Zou, C., Song, J., Wei, S., Peng, P., 2018. Abundances and light absorption properties of brown carbon emitted from residential coal combustion in China. Environ. Sci. Technol. https://doi.org/10.1021/acs.est.8b05630.
Li, M., Fan, X., Zhu, M., Zou, C., Song, J., Wei, S., Peng, P., 2019. Abundance and light absorption properties of Brown carbon emitted from residential coal combustion in China. Environ. Sci. Technol. 53 (2), 595–603. https://doi.org/10.1021/acs.est.8b05630.
Li, X., Sun, N., Jin, Q., Zhao, Z., Wang, L., Wang, Q., Liu, X., 2022. Light absorption properties of black and brown carbon in winter over the North China Plain: impacts of regional biomass burning. Atmos. Environ. 278 https://doi.org/10.1016/j.atmosenv.2022.119100.
Lin, G., Penner, J.E., Flanner, M.G., Sillman, S., Xu, L., Zhou, C., 2014. Radiative forcing of organic aerosol in the atmosphere and on snow: effects of SOA and brown carbon. J. Geophys. Res. Atmos. 119 (12), 7453–7476. https://doi.org/10.1002/2013jd021186.
Liu, J., Bergin, M., Guo, H., King, L., Kotra, N., Edgerton, E., Weber, R.J., 2013. Size-resolved measurements of brown carbon in water and methanol extracts and estimates of their contribution to ambient fine-particle light absorption. Atmos. Chem. Phys. 13 (24), 12389–12404. https://doi.org/10.5194/acp-13-12389-2013.
Liu, J., Kiesewetter, G., Klimont, Z., Cofala, J., Heyes, C., Schopp, W., Amann, M., 2019. Mitigation pathways of air pollution from residential emissions in the Beijing-Tianjin-Hebei region in China. Environ. Int. 125, 236–244. https://doi.org/10.1016/j.envint.2018.09.059.
Luo, J., Zhang, Y., Zhang, Q., 2020. The Ångström exponent and single-scattering albedo of black carbon: effects of different coating materials. Atmosphere 11 (10). https://doi.org/10.3390/atmos11101103.
Luo, L., Tian, H., Liu, H., Bai, X., Liu, W., Liu, S., Zhang, K., 2021. Seasonal variations in the mass characteristics and optical properties of carbonaceous constituents of PM (2.5) in six cities of North China. Environ. Pollut. 268 (Pt B), 115780 https://doi.org/10.1016/j.envpol.2020.115780.
Park, S., Yu, G.-H., Lee, S., 2018. Optical absorption characteristics of brown carbon aerosols during the KORUS-AQ campaign at an urban site. Atmos. Res. 203, 16–27. https://doi.org/10.1016/j.atmosres.2017.12.002.
Pavel, M.R.S., Zaman, S.U., Paul, S., Zaman, P., Salam, A., 2023. Light absorption properties of black carbon and brown carbon emitted from biomass combustion at the typical rural cooking stoves in Bangladesh. Air Quality, Atmosphere & Health. https://doi.org/10.1007/s11869-023-01302-7.
Peng, C., Yang, F., Tian, M., Shi, G., Li, L., Huang, R.J., Chen, Y., 2020. Brown carbon aerosol in two megacities in the Sichuan Basin of southwestern China: light absorption properties and implications. Sci. Total Environ. 719, 137483 https://doi.org/10.1016/j.scitotenv.2020.137483.
Rathod, T.D., Sahu, S.K., 2022. Measurements of optical properties of black and brown carbon using multi-wavelength absorption technique at Mumbai, India. J. Earth Syst. Sci. 131 (1) https://doi.org/10.1007/s12040-021-01774-0.
Retama, A., Ramos-Cerón, M., Rivera-Hernández, O., Allen, G., Velasco, E., 2022. Aerosol optical properties and brown carbon in Mexico City. Environ. Sci.: Atmosphere 2 (3), 315–334. https://doi.org/10.1039/d2ea00006g.
Rizzo, L.V., Artaxo, P., Müller, T., Wiedensohler, A., Paixão, M., Cirino, G.G., Kulmala, M., 2013. Long term measurements of aerosol optical properties at a primary forest site in Amazonia. Atmos. Chem. Phys. 13 (5), 2391–2413. https://doi.org/10.5194/acp-13-2391-2013.
Rizzo, L.V., Correia, A.L., Artaxo, P., Procópio, A.S., Andreae, M.O., 2011. Spectral dependence of aerosol light absorption over the Amazon Basin. Atmos. Chem. Phys. 11 (17), 8899–8912. https://doi.org/10.5194/acp-11-8899-2011.
Shen, H., Huang, Y., Wang, R., Zhu, D., Li, W., Shen, G., Tao, S., 2013. Global atmospheric emissions of polycyclic aromatic hydrocarbons from 1960 to 2008 and future predictions. Environ. Sci. Technol. 47 (12), 6415–6424. https://doi.org/10.1021/es400857z.
Shen, Z., Lei, Y., Zhang, L., Zhang, Q., Zeng, Y., Tao, J., Liu, S., 2017a. Methanol extracted Brown carbon in PM2.5 over xi'an, China: seasonal variation of optical properties and sources identification. Aerosol Science and Engineering 1 (2), 57–65. https://doi.org/10.1007/s41810-017-0007-z.
Shen, Z., Zhang, Q., Cao, J., Zhang, L., Lei, Y., Huang, Y., Zhu, C.J.A.E., 2017b. Optical properties and possible sources of brown carbon in PM2. 5 over Xi'an. China 150, 322–330.
Shen, Z., Zhang, Q., Cao, J., Zhang, L., Lei, Y., Huang, Y., Liu, S., 2017c. Optical properties and possible sources of brown carbon in PM 2.5 over Xi'an, China. Atmos. Environ. 150, 322–330. https://doi.org/10.1016/j.atmosenv.2016.11.024.
Singh, S., Gokhale, S., 2021. Source apportionment and light absorption properties of black and brown carbon aerosols in the Brahmaputra River valley region. Urban Clim. 39 https://doi.org/10.1016/j.uclim.2021.100963.
Sokolik, I.N., Winker, D.M., Bergametti, G., Gillette, D.A., Carmichael, G., Kaufman, Y.J., Penner, J.E., 2001. Introduction to special section: o utstanding problems in quantifying the radiative impacts of mineral dust. J. Geophys. Res. Atmos. 106 (D16), 18015–18027. https://doi.org/10.1029/2000jd900498.
Wang, P., Cao, J.J., Shen, Z.X., Han, Y.M., Lee, S.C., Huang, Y., Huang, R.J., 2015. Spatial and seasonal variations of PM2.5 mass and species during 2010 in Xi'an, China. Sci. Total Environ. 508, 477–487. https://doi.org/10.1016/j.scitotenv.2014.11.007.
Wang, Q., Liu, H., Ye, J., Tian, J., Zhang, T., Zhang, Y., Cao, J., 2020a. Estimating absorption Ångström exponent of black carbon aerosol by coupling multiwavelength absorption with chemical composition. Environ. Sci. Technol. Lett. 8 (2), 121–127. https://doi.org/10.1021/acs.estlett.0c00829.
Wang, Q., Zhou, Y., Ma, N., Zhu, Y., Zhao, X., Zhu, S., Su, H., 2022. Review of Brown carbon aerosols in China: pollution level, optical properties, and emissions. J. Geophys. Res. Atmos. 127 (16) https://doi.org/10.1029/2021jd035473.
Wang, X., Shen, Z., Zeng, Y., Liu, F., Zhang, Q., Lei, Y., Yang, L., 2018. Day-night differences, seasonal variations and source apportionment of PM10-bound PAHs over xi'an, northwest China. Atmosphere 9 (2). https://doi.org/10.3390/atmos9020062.
Wang, Y., Wang, Y., Song, S., Wang, T., Li, D., Tan, H., 2020b. Effects of coal types and combustion conditions on carbonaceous aerosols in flue gas and their light absorption properties. Fuel 277. https://doi.org/10.1016/j.fuel.2020.118148.

Xie, M., Chen, X., Hays, M.D., Holder, A.L., 2019. Composition and light absorption of N-containing aromatic compounds in organic aerosols from laboratory biomass burning. Atmos. Chem. Phys. 19 (5), 2899–2915. https://doi.org/10.5194/acp-19-2899-2019.

Xie, X., Chen, Y., Nie, D., Liu, Y., Liu, Y., Lei, R., Ge, X., 2020. Light-absorbing and fluorescent properties of atmospheric brown carbon: a case study in Nanjing, China. Chemosphere 251, 126350. https://doi.org/10.1016/j.chemosphere.2020.126350.

Yan, F., Kang, S., Sillanpaa, M., Hu, Z., Gao, S., Chen, P., Li, C., 2020. A new method for extraction of methanol-soluble brown carbon: implications for investigation of its light absorption ability. Environ. Pollut. 262, 114300 https://doi.org/10.1016/j.envpol.2020.114300.

Yan, J., Wang, X., Gong, P., Wang, C., Cong, Z., 2018. Review of brown carbon aerosols: recent progress and perspectives. Sci. Total Environ. 634, 1475–1485. https://doi.org/10.1016/j.scitotenv.2018.04.083.

Yao, L., Yang, L., Yuan, Q., Yan, C., Dong, C., Meng, C., Wang, W., 2016. Sources apportionment of PM2.5 in a background site in the North China Plain. Sci. Total Environ. 541, 590–598. https://doi.org/10.1016/j.scitotenv.2015.09.123.

Zeng, Y., Shen, Z., Takahama, S., Zhang, L., Zhang, T., Lei, Y., Rudolf, H., 2020. Molecular absorption and evolution mechanisms of PM2.5 Brown carbon revealed by electrospray ionization fourier transform–ion cyclotron resonance mass spectrometry during a severe winter pollution episode in xi'an, China. Geophys. Res. Lett. 47 (10) https://doi.org/10.1029/2020gl087977.

Light absorption properties of brown carbon aerosol after coal to natural gas switch policy in China: a case study in winter $PM_{2.5}$ over Xi'an, northwestern China

Yukun Chen[1]; Yongwei Lu[1]; Ting Wang[1,2]; Jukai Chen[1,3]; Yueshe Wang[1,*]; Eric Lichtfouse [1,4]

[1] State Key Laboratory of Multiphase Flow in Power Engineering, Xi'an Jiaotong University, Xi'an 710049, China;

[2] Xi'an Aeronautics Computing Techniques Research institute, , Xi'an 710068, China;

[3] School of Chemical Engineering & Technology, China University of Mining and Technology, Xuzhou 221116, PR China;

[4] Aix-Marseille University, CNRS, IRD, INRA, Coll France, CEREGE, Aix-en-Provence 13100, France.

Correspondence to:
[*]Yueshe Wang (wangys@mail.xjtu.edu.cn; Tel.: +029-8266-7323).

Sampling site

Figure S1 shows the detailed information about the sampling location in the campus of Xi'an Jiaotong University in our study, which is marked in red color in Fig. S1.

Figure S1. Location of the sampling site in Xi'an Jiaotong University.

$PM_{2.5}$ mass concentration

The mass concentration of the $PM_{2.5}$ sampling was obtained by analyzing the filters gravimetrically using an electronic microbalance with a sensitivity of ± 0.001 mg (Sartorius, Germany). Before weighing, the sample filters were equilibrated in a container with the temperature of about 26 °C and the relative humidity of 35% for 24 hours. Each filter was weighed in triplicate before and after sampling. The net mass was obtained by subtracting the average of the pre-sampling weights from the average of the post-sampling weights.

Water-soluble ions

A quarter (about 4.34 cm^2) of a sample filter membrane was cut to analyze water-soluble ions. The cut portion was immersed in a 50 mL ultrapure water (18.2 MΩ), then was oscillated for 15 min followed by 15-min sonication. This procedure was repeated four times at least. The mixture processed by the above procedure was then filtered through a syringe filter membrane, where the pore size is around 0.22 μm, and

the extracted solution was stored in a freezer before analysis. Five cations ($NH4^+$, Na^+, K^+, Mg^{2+}, Ca^{2+}) and four anions (SO_4^{2-}, NO_3^-, NO_2^-, Cl^-) in the extract were analyzed by two ion chromatography instruments (i.e., DionexIntegrion, US and RPIC-2019, Ruipu, China), respectively.

Carbonaceous fractions

A punch (0.52 cm^2) of each sample was taken to measure the content of organic carbon (OC) and EC using a Thermal/Optical Carbon Analyzer (Model DRI 2001A) following the IMPROVE-TOR temperature protocol (Cao et al., 2003; Chow et al., 2004; Chow et al., 1993). Four OC fractions (OC1, OC2, OC3, and OC4 at 140, 280, 480, and 580 ^{0}C respectively, in a 100% He atmosphere), a optically detected pyrolyzed carbon fraction (OPC, the amount of carbon measured after oxygen is added until the reflectance achieves its original value), and three EC fractions (EC1, EC2, and EC3 at 580, 740, and 840 ^{0}C respectively, in a 98% He/2% O2 atmosphere) were determined in this study. OC was defined as OC1 + OC2 +OC3 +OC4 +OPC and EC was EC1 + EC2 + EC3 – OP (Cao et al., 2003).

WSOC and MSOC measurement

Water-soluble organic carbon (WSOC) extracts were obtained following the same procedure as the above pretreatment of water-soluble ions. The WSOC concentration was determined by a TOC/TNB analyzer (Total Organic Carbon Total Nitrogen Analyzer, vario, Element, Germany).

Methanol-soluble organic carbon (MSOC) extracts were obtained following the method established by Cheng (Cheng et al., 2016) with minor modification. Briefly, a punch (0.52 cm^2) of each filter sample was first immersed in 100 mL methanol for an hour. The filter was then removed from methanol and baked for 30 min in an oven at 50 ^{0}C. After that, the punch was analyzed by the Thermal/Optical Carbon Analyzer. The MSOC content can be calculated by the following Eq.S1:

$$MSOC=OC_{untreated}-OC_{extracted}, \quad (S1)$$

where $OC_{untreated}$ and $OC_{extracted}$ are the OC concentrations of the untreated (OC concentration obtained in section 2.2.3) and extracted (OC concentration obtained in section 2.2.4) samples, respectively. Four pairs of untreated and extracted blank filters were measured by the Thermal/Optical Carbon Analyzer as well. The concentration of OC in untreated and extracted blank filters was range from 0.41 μg C cm^{-2} to 0.56 μg C cm^{-2} (all are under the Method Detection Limit, which is 0.82 μg C cm^{-2}), indicating negligible contamination during the extracting and drying processes.

Source apportionment of BrC in WSOC and MSOC

The sources apportionment of $PM_{2.5}$ and their contribution to OC in winter of Xi'an are shown in Fig.S2. There are five emission sources resulting in the pollution episodes, which are the biomass burning, motor vehicle emission, coal combustion, dust and secondary source, respectively.

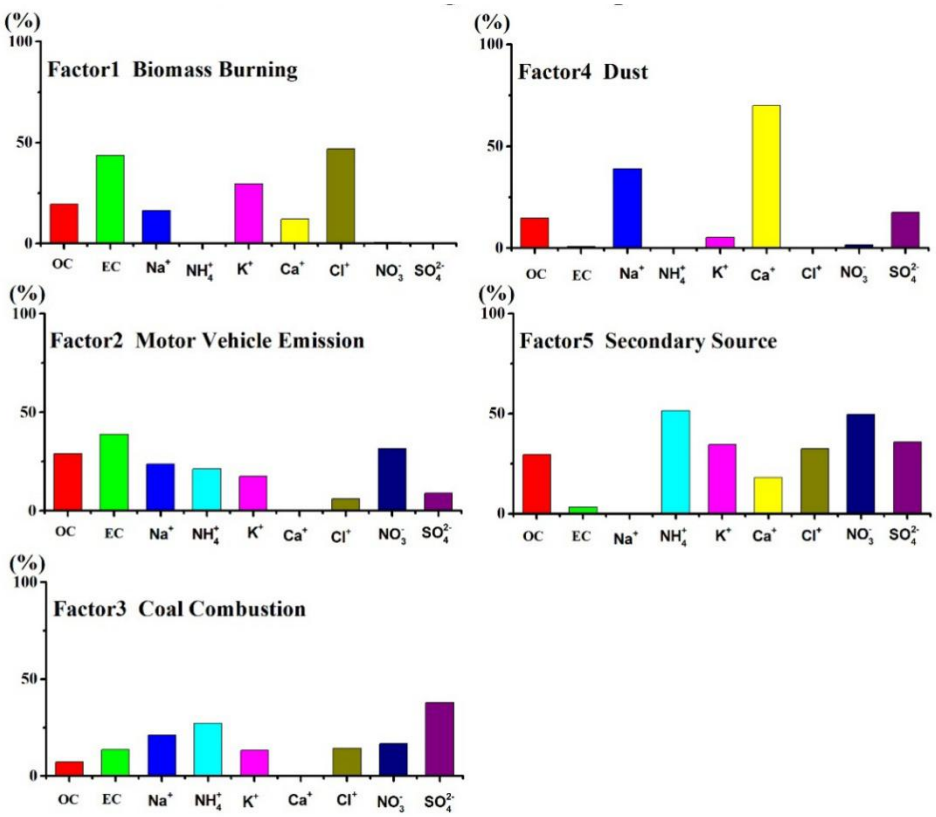

Figure S2. Five main source emissions identified by PMF. Factor 1 to factor 5 represent biomass burning, motor vehicle emission, coal combustion, dust and secondary sources, respectively.

Factor 1 is identified to be the biomass burning source. The representative species are highest mass concentration of K^+ (29.67%) and Cl^-(46.84%) and EC (43.69%), as well as a medium mass concentration of OC (19.52%). In winter of Xi'an, residence heating, the 'heating Kang' in the rural, agricultural burning, as well as cooking are the different biomass burning lead to the emission of OC and also produce the representation of incomplete burning as EC. What's more, K^+ and Cl^- are also the characterization of straw burning or smoldering. Further, biomass burning always accompanies with the secondary organic aerosol (SOA), which can produce a lot of OC (Chen et al., 2018; Qiu et al., 2019; Yao et al., 2016). Shen et al(Shen et al., 2017) proved that there is a good synergy between the mass concentration of K^+ and the Abs of BrC in WSOC over Xi'an, which is consistent with our results(Fig.4).So the biomass burning is an important source for BrC.

Factor 2 is the motor vehicle emission with the relatively high concentrations of EC (38.83%) and a medium level of NO_3^-(31.71%) with OC (29.12%). Yao et al (2016) indicated that both diesel and gasoline combustion can generate large amounts of OC, EC and NOx. Also, the positive correlation coefficient *r* between Abs_{365} and NO_3^- as well as EC in Fig.4 demonstrates motor vehicle emission is a primary contributor to BrC.

Because of a large portion of SO_4^{2-}(37.90%) and a medium level of Na^+ (21.07%), we classify Factor 3 as the coal combustion source. The sulfur content in raw coal is relatively high, so the emission of SO_2 may be high resulting in the secondary transformation to SO_4^{2-}. Na^+ is also an appropriate characterization of coal combustion. In addition, the content of OC is less than that in other sources and the contribution of EC is relatively lower, where may attribute to the implementation of the ban of coarse coal burning sites at the end of 2017, Xi'an. Combining Fig.4, we conclude that the contribution of coal combustion is just a small fraction to light absorption properties of BrC after the policy of abrogating the coarse coal burning.

Factor 4 is identified to the dust source with the highest mass concentration of Ca^{2+} (69.96%) and Na^+ (38.94%). Due to the special topography of Xi'an, the dust storms from the northwest regions may also be an chief portion of BrC to compose $PM_{2.5}$. And the content of EC (0.70%) is relatively less than that in other factors. It may be due to the deposition of coarse particulate matter. As a part of fine organic aerosols, dust also have an effect on the light absorption of $PM_{2.5}$(Rogge et al., 1993; Yang et al., 2009).

Due to the highest mass concentration of NH_4^+ (51.51%), NO_3^-(49.52%), SO_4^{2-} (35.73%). Factor 5 we identified is the secondary source. What we concerned is that the concentration of EC is near to 0. Because EC is derived from primary emission sources, this factor is consistent with the secondary emission. The parent substances of these representatively inorganic ions are SO_X and NO_X, and can be derived from the primary emissions, such as high vehicular emissions in winter of Xi'an. Then these parent substances have a fast secondary formation in atmosphere (Kim et al., 2016; Kirillova et al., 2014; Yang et al., 2009; Yuan et al., 2014), becoming $(NH_4)_2SO_4$, NH_4HSO_4 or NH_4NO_3(Zhang et al., 2011) to produce more sever pollution in winter.

Table S1. Comparison of absorption coefficient (*Abs*), mass absorption coefficient (*MAE*) at 365nm and Absorption Angstrom coefficient (*AAE*) values of brown carbon from the ambient particle 2.5 in winter between the present and earlier studies.

Region	Sampling Date	Species	Abs_{365} (Mm^{-1})	MAE_{365} ($m^2\ g^{-1}$)	*AAE*	Reference
Xi'an, China	2018.11.15-2018.12.25	Methanol/Water-Soluble BrC	MSBrC：33.0±17.1	2.5±0.6	6.8	This Study
			WSBrC：17.8±9.6	2.0±0.6	6.1 (330-550nm)	
Xi'an, China	2017.1.1-2017.1.6	Methanol-Soluble BrC	42.0±18.1	1.2±0.2	6.2±0.5（330-400nm）	Lei et al 2019
Xi'an, China	2008.11.15-2009.3.14	Methanol/Water-Soluble BrC	MSBrC：46.±20.3	1.33±0.34	6.0±0.2	Huang et al 2018
			WSBrC：25.2±11.6	1.65±0.3	5.7 (330-550nm)	

				6		
Beijing, China	2011.12.7-2011.12.31	Methanol/Water-Soluble BrC	MSBrC：26.20±18.81 WSBrC：10.22±6.93	1.45±0.26 1.22±0.11	7.10±0.45 7.28±0.24 (310-450nm)	Cheng et al 2015
Beijing, China	2010.10-2013.9	Water-Soluble BrC	10.1±8.6	1.26	7.5 (300-700nm)	Du et al 2014
Beijing, China	2009 winter	Water-Soluble BrC	_	1.79±0.24	7.5±0.9 (330-480nm)	Cheng Y and He K-B et al 2011
Shenzhen, China	2014.1.15-2014.2.19	Water-Soluble BrC	3.0 (405nm) 1.9 (532nm)	_	1.7 (405-532nm)	Yuan J-F et al 2016
Indo-Gangetic Plain (Northern India)	Winter（11.9-3.10）	Water-Soluble BrC	2-21	0.78±0.24	6.0±1.1 (300-700nm)	Bikkina Srinivas et al 2014
South Dekalb	2007 winter	Water-Soluble BrC	_	0.60±0.23	6.0 for March 7th 7.4 for November 8th	Hecobin et al 2010
Yorkville	2007 winter	Water-Soluble BrC	_	0.63±0.31	7.8 for March 1st 7.2 for December 20th	
Bay of Bengal (IGP-outflow)	2008.12.27-2009.1.10（PM10）	Water-Soluble BrC	_	0.4±0.1	9.1±2.5	Srinivas and Sarin et al 2013
Bay of Bengal (IGP-outflow)	2008.12.27-2009.1.10（PM10）	Water-Soluble BrC	_	0.5±0.2	6.9±1.9	
Xiamen,	2014.1.1-2014.	Water-Soluble	59.4	_	1.52±0.02	Qiu et al

China	12.31	BrC	(370nm)		(370-880nm)	2019
Nanjing, China	2015.5-2016.5	Water-Soluble BrC	9.44±4.70	1.04	6.74 (300-600nm)	Chen et al 2018
Xi'an, China	2010.11.2-2011.2.24	Water-Soluble BrC	36.2 (340nm)	5.8 (340nm)	5.7	Shen et al 2017
Hebei, China	2005.302-2005.3.26	Water-Soluble BrC	_	2.2 (370nm)	3.5 (470-660nm)	Yang M et al 2009
Seoul, Korea	2012.10-2011.11	Methanol/Water-Soluble BrC	MSBrC：10.93	0.85	5.54	Kim Hwajin et al 2016
			WSBrC：7.31±2.52	1.02	5.84 (300-700nm)	
Goson, Korea	2011.3.8-2011.3.27	Water-Soluble BrC	_	0.7±0.2	6.4±0.6 (330-400nm)	E.N.Kirillova et al 2014
Beijing, China	2013.1-2013.6	Water-Soluble BrC	_	1.43±0.36	6.19±0.43 (340-400nm)	Yan et al 2017
Yulin, China	2015.12.19-2016.1.1	Methanol/Water-Soluble BrC	MSBrC：27.5±12.0	1.4±0.4	4.9±1.2	Lei et al 2018
			WSBrC：8.9±4.9	_	5.2±0.8 (330-400nm)	
Guangzhou, China	2012.12.13-2012.12.27（TSP）	Water-Soluble BrC	3.57±1.34	0.81±0.16	5.33±0.71 (310-450nm)	Liu et al 2018

Note:

The MSBrC means the methanol-soluble BrC, and WSBrC means the water-soluble BrC.

All the data are from the literature or calculated by the public data.

"_" means not measured or determined.

Reference

Cao, J. J., Lee, S. C., Ho, K. F., Zhang, X. Y., Zou, S. C., Fung, K., & Watson, J. G. (2003). Characteristics of carbonaceous aerosol in Pearl River Delta Region, China during 2001 winter period. *Atmospheric Environment*, *37*, 1451-1460, http://doi.org/10.1016/S1352-2310(02)01002-6.

Chen, Y., Ge, X., Chen, H., Xie, X., Chen, Y., Wang, J., & Chen, M. (2018). Seasonal light absorption properties of water-soluble brown carbon in atmospheric fine particles in Nanjing, China. *Atmospheric Environment*, *187*, 230-240, http://doi.org/10.1016/j.atmosenv.2018.06.002.

Cheng, Y., He, K. B., Du, Z. Y., Engling, G., Liu, J. M., Ma, Y. L., & Weber, R. J. (2016). The characteristics of brown

carbon aerosol during winter in Beijing. *Atmospheric Environment*, *127*, 355-364, http://doi.org/10.1016/j.atmosenv.2015.12.035.

Chow, J. C., Watson, J. G., Chen, L. W. A., W Patrick, A., Hans, M., & Kochy, F. (2004). Equivalence of elemental carbon by thermal/optical reflectance and transmittance with different temperature protocols. *Environmental Science & Technology*, *38*(16), 4414-4422, http://doi.org/10.1021/es034936u.

Chow, J. C., Watson, J. G., Pritchett, L. C., Pierson, W. R., Frazier, C. A., & Purcell, R. G. (1993). The dri thermal/optical reflectance carbon analysis system: description, evaluation and applications in U.S. Air quality studies. *Atmos Environ A*, *27*(8), 1185-1201, http://doi.org/10.1016/0960-1686(93)90245-T.

Kim, H., Kim, J. Y., Jin, H. C., Lee, J. Y., & Lee, S. P. (2016). Seasonal variations in the light-absorbing properties of water-soluble and insoluble organic aerosols in Seoul, Korea. *Atmospheric Environment*, *129*, 234-242, http://doi.org/10.1016/j.atmosenv.2016.01.042.

Kirillova, E. N., Andersson, A., Tiwari, S., Srivastava, A. K., Bisht, D. S., & Gustafsson, Ö. (2014). Water-soluble organic carbon aerosols during a full New Delhi winter: Isotope-based source apportionment and optical properties. *Journal of Geophysical Research: Atmospheres*, *119*(6), 3476-3485, http://doi.org/10.1002/2013jd020041.

Qiu, Y., Wu, X., Zhang, Y., Xu, L., Hong, Y., Chen, J., & Deng, J. (2019). Aerosol light absorption in a coastal city in Southeast China: Temporal variations and implications for brown carbon. *J Environ Sci (China)*, *80*, 257-266, http://doi.org/10.1016/j.jes.2019.01.002.

Rogge, W. F., Hildemann, L. M., Mazurek, M. A., Cass, G. R., & Simoneit, B. R. T. (1993). Sources of fine organic aerosol. 3. Road dust, tire debris, and organometallic brake lining dust: roads as sources and sinks. *Environ.sci.technol*, *27*(9), 1892-1904, http://doi.org/10.1021/es00046a019.

Shen, Z., Zhang, Q., Cao, J., Zhang, L., Lei, Y., Huang, Y., & Liu, S. (2017). Optical properties and possible sources of brown carbon in PM 2.5 over Xi'an, China. *Atmospheric Environment*, *150*, 322-330, http://doi.org/10.1016/j.atmosenv.2016.11.024.

Yang, M., Howell, S., Zhuang, J., & Huebert, B. (2009). Attribution of aerosol light absorption to black carbon, brown carbon, and dust in China–interpretations of atmospheric measurements during EAST-AIRE. *Atmospheric Chemistry and Physics*, *9*(6), 2035-2050, http://doi.org/10.5194/acpd-8-10913-2008.

Yao, L., Yang, L., Yuan, Q., Yan, C., Dong, C., Meng, C., & Wang, W. (2016). Sources apportionment of PM2.5 in a background site in the North China Plain. *Sci Total Environ*, *541*, 590-598, http://doi.org/10.1016/j.scitotenv.2015.09.123.

Yuan, Q., Yang, L., Dong, C., Yan, C., Meng, C., Sui, X., & Wang, W. (2014). Temporal variations, acidity, and transport patterns of PM2.5 ionic components at a background site in the Yellow River Delta, China. *Air Quality, Atmosphere & Health*, *7*(2), 143-153, http://doi.org/10.1007/s11869-014-0236-0.

Zhang, T., Cao, J. J., Tie, X. X., Shen, Z. X., Liu, S. X., Ding, H., & Li, W. T. (2011). Water-soluble ions in atmospheric aerosols measured in Xi'an, China: Seasonal variations and sources. *Atmospheric Research*, *102*(1-2), 110-119, http://doi.org/10.1016/j.atmosres.2011.06.014.